Effect of line and trench profile variation on specular and diffuse reflectance from a periodic structure

Thomas A. Germer

Optical Technology Division, National Institute of Standards and Technology,

Gaithersburg, Maryland 20899

We investigate the effects that variations in profile have on specular reflectance and polarization from a grating consisting of parallel lines or trenches. We model the effects of variations by calculating the reflectance of a superstructure, in which the profiles are randomly modulated about their nominal profile. We investigate, as an example, a nominal grating consisting of 100 nm silicon lines having a vertical sidewall angle, a pitch of 200 nm, and a height of 100 nm probed with a wavelength of 532 nm. We vary the edge positions, the edge profiles, the line heights, and the trench depths and find that the Stokes reflectance can be modified from its nominal value by a relatively large amount, especially in the case of line-width variations. We find that the reflected field can be approximated by the mean field reflected by a distribution of periodic gratings and that the field does not represent the field from the average profile. When fitting results to more than one modeled parameter, the changes that are observed can be enough to shift the deduced parameter in some cases by more than the rms variation of that parameter. The diffuse

reflectance (the non-specular diffraction efficiency) is found to increase with the variance of the fluctuations.

OCIS Codes: 050.0050, 120.2130, 120.3930, 290.3700

1. Introduction

The reflectance of a periodic array of lines on a surface can be very sensitive to the profile of that structure. The semiconductor industry has capitalized on this sensitivity to measure line widths and profiles of micro-fabricated structures.[1,2,4,5,8-10,12] Measurements generally consist of recording the reflectance or polarization as a function of incident angle or wavelength from a periodic test structure. Comparison of the measurement with a library of simulated results for a variety of different possible profiles yields the one which matches the data best. The technique has been dubbed *scatterometry* in the industry, although rarely does it make use of the diffusely scattered light or anything but the specular reflectance.

While the method is extremely sensitive to details of the profile, comparisons between scatterometry instruments and other metrology methods have not yielded ideal agreement.[11] One of the assumptions that is generally made in the interpretation of data is that the structure is indeed periodic, and that any deviation from periodicity gives the same result as some "average" profile. In this article, we investigate the validity of this assumption by performing Monte Carlo (MC) simulations on extended gratings with randomized profiles. We find that deviations from periodicity do not give the same result as the field from the average profile, but rather that the reflected field can be approximated by the mean field reflected by a distribution of periodic

profiles. Furthermore, the best fit simple profile to the MC simulated data can be shifted by a large amount from that predicted by the average profile.

In Section 2, we outline the theoretical approach used to perform the MC simulations and describe a mean-field model used to approximate the results. In Section 3, we present the results of those simulations and discuss them. Finally, in Section 4, we draw some conclusions from this work.

2. Theory

A. Grating Simulations

We use the rigorous coupled wave (RCW) analysis for surface relief gratings developed by Moharam, *et al.*,[6,7] with a modification suggested by Lalanne and Morris[3] to improve the convergence of the calculations for transverse-magnetic (TM) polarization. This method solves the electromagnetic problem for a plane wave incident upon a medium having a dielectric function $\varepsilon(x, y, z) = \varepsilon_j(x)$, which is periodic in *x*, independent of *y*, and independent of *z* within each of a finite number of layers, indicated by index *j*. The solution requires Fourier series expansions of $\varepsilon_j(x)$ and $1/\varepsilon_j(x)$ for each layer. In practice, the Fourier series is truncated at some maximum order *N*. We generally chose *N* so that the shortest period of the Fourier component considered is 10 nm.

B. Monte Carlo Simulations

We begin by considering an unperturbed grating having a period Λ_0. To simulate variations in the profile, we create random profiles having a total period $\Lambda_M = M\Lambda_0$ (*M* an integer) and solve

for the scattering amplitude using the RCW method on this larger period. Generally, the unperturbed grating gives rise to diffraction at discrete directions, given by

$$\sin\theta_i = \sin\theta + i\lambda/\Lambda_0, \tag{1}$$

where θ is the incident angle, θ_i is the diffracted angle, and λ is the wavelength of the light. The simulated profiles having the longer period give rise to diffraction at additional directions, such that *i* takes on fractional values (*i.e.*, *iM* is an integer). We will denote these fractional orders as *diffuse* orders, since they do not exist for the primary period, and as *M* increases, the number of these orders expands into a diffuse continuum as would be expected from a non-periodic structure.

We consider four different perturbations of the profile, illustrated in Fig. 1. In the first case [Fig. 1(a)], we consider variations in the line edge position. We let Δx_j^L and Δx_j^R be deviations of the left and right edges of the *j*-th line. We create realizations of the random profile, using a pseudo-random number generator having a normal distribution with standard deviation σ. We further consider three different sub-cases of line edge variation. For *line position variation*, we let $\Delta x_j^L = \Delta x_j^R$; for *line width variation*, we let $\Delta x_j^L = -\Delta x_j^R$; and, for *random edge variation*, we let Δx_j^L and Δx_j^R be independent. In all calculations for the simulation of line edge variation, since the side walls are vertical, only one *z*-level is required in the RCW calculation.

The second profile perturbation corresponds to sidewall roughness [Fig. 1(b)]. In this case, the profile of the sidewall consists of realizations of a random function having an rms roughness σ and correlation length τ. Realizations of the random function are generated by

$$\Delta x(z) = \mathrm{Re}\frac{1}{\pi\sqrt{2}}\int \mathrm{d}k \int \mathrm{d}z'\, g(z') \exp[\mathrm{i}\phi(k) + \mathrm{i}k(z - z')] \tag{2}$$

where $\phi(k)$ is a uniform random function with interval (0,2π], and

$$g(z) = A\exp[-(z/\tau)^2/2] \tag{3}$$

is the correlation function. A is adjusted to yield a specific rms roughness. Eq. (2) is derived from a Fourier transform of the correlation function, multiplication by a random phase, followed by an inverse Fourier transform. For a finite interval, L, over which a realization of the function is calculated, A is given by

$$A = \sigma\pi^{1/4}(L/\tau)^{1/2}\,\mathrm{erf}\,(L/2\tau)\,. \tag{4}$$

Like the case of line edge position variation, we consider three different sub-cases, analogous to line position, line width, and random edge variation. Line-edge variation is a special case of sidewall roughness, where $\tau \gg L$. For all simulations of sidewall roughness, the profile was subdivided into 50 levels. The only correlation length considered was $\tau = 10$ nm.

The third profile perturbation considered is that of *line height variation* [Fig. 1(c)]. Here we use a pseudo-random number generator having a normal distribution with standard deviation σ to sample the perturbation of the height of each line of the grating. To perform the RCW calculation for M lines, we divide the grating into M discrete z-levels. We sample the M heights Δz_j from the distribution, sort the values in ascending order, and use the differences between heights to determine the thickness of each level. Each level only contains the lines which extend to that level.

The fourth, and final, profile perturbation is that of *trench depth variation* [Fig. 1(d)]. The simulation for trench depth variation is performed in a manner analogous to that used for line height variation.

For each case, MC simulations were performed for at least 40 realizations of the surface profile. The mean and the standard error for each measurable parameter were found. We used M = 10 lines for each realization, except in the case of sidewall roughness, where we used M = 5 lines, to compensate for the larger number of layers needed and the resulting additional computation time. The nominal pitch Λ_0 was 200 nm, the nominal height was 200 nm, and the nominal width was 100 nm. The optical constants of the grating material and the substrate were those appropriate for silicon. The wavelength was 532 nm, where the optical constants are n = 4.05 and k = 0.05, unless otherwise noted.

Simulations were performed for two incident orthogonal polarizations at normal incidence and 70° incidence perpendicular to the lines. The Stokes parameters for incident light linearly polarized at an angle of 45°,

$$\begin{aligned} R_0 &= \tfrac{1}{2}\left|r_{\mathrm{TE}}\right|^2 + \tfrac{1}{2}\left|r_{\mathrm{TM}}\right|^2 \\ R_1 &= \tfrac{1}{2}\left|r_{\mathrm{TE}}\right|^2 - \tfrac{1}{2}\left|r_{\mathrm{TM}}\right|^2 \\ R_2 &= \mathrm{Re}\, r_{\mathrm{TE}}^{\,*} r_{\mathrm{TM}} \\ R_3 &= \mathrm{Im}\, r_{\mathrm{TE}}^{\,*} r_{\mathrm{TM}} \end{aligned} \tag{5}$$

are presented, where r_{TE} and r_{TM} are the reflectance coefficients for light polarized with the electric field and magnetic fields along the lines, respectively. Simulations in a conical geometry with 70° incidence along the lines were also performed, but the conclusions do not differ from the others, and the results are not shown.

C. Mean Field Model

We compared the MC simulation results to those of an approximate model to answer the question of whether or not the field reflected by a random pattern is the average of the field reflected by a distribution of periodic patterns. If the scattering by the lines is dominated by the structure of each individual line, rather than by line-line interactions, then we would expect this statement to be true. If we consider the field scattered by a periodic array of lines having parameter *a* (height, depth, width, or period) to be $\mathbf{E}(a)$, then the field averaged over a normal distribution of the parameter *a* is given by

$$\langle \mathbf{E} \rangle_a = \frac{1}{\sigma_a \sqrt{2\pi}} \int \mathrm{d}a \, \mathbf{E}(a) \exp[-(a - a_0)^2 / 2\sigma_a{}^2] \tag{6}$$

where a_0 and σ_a are the mean and standard deviation of *a*, respectively. Since the RCW theory references the field to the top of the lines, variations in line height and line depth differ by the introduction of an additional phase term

$$\mathbf{E}(h) = \mathbf{E}(d) \exp(-2\mathrm{i}k_z d) \tag{7}$$

where $k_z = (2\pi / \lambda) \cos\theta$ is the *z*-component of the wavevector. For variations in line width or period, since the parameter σ is the rms variation of a single edge, it must be borne in mind that comparisons between the Monte Carlo models must be performed such that $\sigma_{\text{linewidth}} = \sigma\sqrt{2}$ for random edge variation, $\sigma_{\text{linewidth}} = 2\sigma$ for line width variation, and $\sigma_{\text{period}} = \sigma / \sqrt{2}$ for line position variation. Eq. (6) is evaluated by numerical integration, sampling the electric field at discrete points. The mean field model is attractive, if it proves to be accurate, because

simulations required to evaluate Eq. (6) are performed anyways during construction of a scatterometry library.

3. Results and Discussion

Figures 2 and 3 show results for the specular Stokes reflectance obtained from the MC simulations for line edge variation and sidewall roughness. Results from both MC simulations (symbols) and the mean field model (curves) are shown. It is apparent that line variation has a relatively large effect on the reflectance of the grating. Changes in the Stokes parameters correspond, for example, to fractional changes in the *p*-polarized reflectance, $R_p = R_0 - R_1$, of almost 50 %, over the range of variations studied, even though the average profile is fixed and the rms variations are less than 2 % of the wavelength.

To assess the magnitude of these results and how they might translate into errors in the dimensions extracted from data, the four MC-simulated Stokes parameters were least-squares fitted to those calculated for simple profiles (i.e., with period Λ_0), letting line width and line height be free parameters. It was found, for example, that for random edge variation measured at normal incidence [i.e., Fig. 2(a), open symbols], the best fit line height decreased at a rate of approximately three times the rms variation, and the best fit line width increased at a rate of approximately two times the rms variation. Some of this unexpectedly large effect is due to the large covariance between line height and line width and to the small number of data points (4) versus the number of fitting parameters (2). While we are varying only line edge position, we are comparing the MC results to simulations where we vary both line width and line height. Thus, the line height compensates for the fact that the mean Stokes parameters do not correspond to those for a simple profile with the same height. Most scatterometry instruments do not perform

measurements at a single wavelength and angle but rather use a scan over one of these variables. Thus, the specific example we give may not be representative of a realistic scatterometry measurement. However, this simple comparison does suggest that variations in line profile can have an adverse effect in the profile determination, if variations in that profile are not considered. Later, we discuss results where we MC simulate a wavelength scan.

The effects of sidewall roughness, shown in Figs. 2 and 3 as closed symbols, are very similar to those obtained for line edge variation. Since the sidewall roughness considered and line edge variation represent two extremes in correlation length of sidewall roughness, we conclude that the correlation length has a relatively weak effect on the reflectance.

The effects of line width variation are much stronger than that observed for incoherent line edge variation, which in turn are much stronger than that observed for line position variation. In fact, a change in the abscissa for the random edge variation results by a factor of about $\sqrt{2}$ maps them onto the results for line width variation. These observations suggest the reflection properties, at least for this particular grating, are dominated by the size of the features rather than the space between them and that the mean-field model would be an appropriate approximation.

The results for the simplified mean-field model are shown as curves in Figs. 2 and 3, where variations in line width were considered [*i.e.*, *a* in Eq. (6) was line width]. Most of the trends observed in the MC results are reproduced, but there is not a perfect match between them. Presumably, differences between the mean-field model and the MC results must be a result of differences in the line widths between adjacent lines having an effect on the reflection properties. The case of line edge roughness matches the model quite well, while the corresponding case of sidewall roughness does not match well at all, showing a much larger dependence upon rms

variation. While the models do not match perfectly, the fact that the calculations required to evaluate Eq. (6) are performed anyway during the construction of a scatterometry library may make the mean-field model attractive for approximating the effect of line edge variations, line width variations, or sidewall roughness.

Figures 4 and 5 show the results for line height and trench depth variations. The effects are less pronounced than for line edge variation, but nonetheless significant. The qualitative agreement between the MC simulations and the mean-field model is also similar to that observed for line edge variation. In this case, variations in trench depth were considered [*i.e.*, *a* in Eq. (6) was trench depth], and the phase was appropriately adjusted for the case of line height variation, as described above.

Figure 6 shows the integrated diffuse reflectance, calculated by summing all of the non-specular diffraction efficiencies, for line edge variation and sidewall roughness at normal incidence. Because the super-period Λ_M chosen was different, there were six orders (i = ±1, ±2, and ±3) summed in the case of line edge variation while only two orders (i = ±1) summed in the case of sidewall roughness. The results show a characteristic proportionality between the integrated diffuse reflectance and the variance parameter σ^2. In all cases, the diffuse reflectance is too small to account for any changes in the specular reflectance. However, the diffuse scatter for line position variation is significantly less than that for other cases of line variation, which is in agreement with changes that are found to occur in the specular reflectance. Table 1 shows the fraction of the total diffracted light diffracted into each of the orders for the three cases of line edge variation. While only three orders appear on each side of the surface normal in these simulations, the results in Table 1 suggest that the angular distribution of diffusely scattered light would be very different for the different cases of line edge variation, at least in the case where

there are no line-to-line correlations. Line-to-line correlations would be expected to further affect the distribution of diffusely scattered light.

Figure 7 shows the MC-simulated normal incidence Stokes reflectance of the structure for wavelengths from 250 nm to 600 nm for the case of random edge variation with σ = 10 nm. The behavior of the nominal structure, shown as solid curves, does not approximate well the behavior for the MC-simulation, shown as symbols, showing shifts in some regions of the spectrum and significantly more structure. The predictions of the mean field approximation, shown as dashed curves, are much closer to the MC simulation of the perturbed profile, especially at shorter wavelengths. At longer wavelengths, correlations between lines ought to become important, so that the mean field model would fail, but it is still a much better match to the perturbed structure than that calculated for the nominal, unperturbed grating.

A least-squares best fit of the MC-simulated results to a simple profile (i.e., with period Λ_0), letting the line width and line height be free parameters, yielded a width of 98.9 nm and a height of 198.8 nm. The observed shift, 1.1 nm in width and 1.2 nm in height, is much smaller than that found for the single Stokes fit described above. The best fit curves were only slightly better than those for the nominal profile, with an improvement in the mean-square deviation of only 5 %. A fit to a simple profile with an angled sidewall, letting the top width, bottom width, and height be free parameters, yielded a top width of 95 nm, a bottom width of 105 nm, and a height of 200 nm. While a slightly better fit (see Fig. 7, dotted curves) to the MC-simulation than that for the simpler profile, the improvement in the mean-square deviation compared to that of the nominal profile was still small, only 15 %. Both fits only searched for the nearest local minimum in the mean-square deviation and did not search for a global minimum. However, it is

clear that with multiple fitting parameters, significant systematic errors can result from the neglect of the profile variation.

This study only investigated the effects of line profile shape and did not consider variations in that profile along the *y* direction. The latter variations are commonly referred to as line-edge roughness (LER) and line-width roughness (LWR) when the position and width vary along the line, respectively. LER and LWR are considered important to microfabrication because they may have an effect on device performance and limit the precision of critical-dimension scanning electron microscopy (CD-SEM). The effects of LER and LWR on specular diffraction might be expected to follow those of line position variation and line width variation, provided the correlation length of the roughness in the *y* direction is significantly larger than the period. It waits to be seen, until full three-dimensional simulations are performed, what the effects are of short correlation length roughness.

In all of the MC simulations that were performed, there were no line-to-line correlations. The matching of the mean-field model to the MC-simulated results would be expected to be better if correlations between neighboring lines were higher. Higher line-to-line correlations would be expected in the cases of line height and line depth variations, because, in practice, these originate from non-uniform etching, deposition, or coating, or roughness of the initial material. However, the cases of line edge variation, line width variation, and sidewall roughness tend to be uncorrelated from line to line, except at distances larger than those typically used for scatterometry targets (50 µm to 100 µm), because the mechanisms that lead to the small distance correlations are usually related to the photoresist structure, while those that lead to the large distance variations are usually related to focus and exposure.

4. Conclusions

This article described some Monte Carlo simulations of reflection and scattering by randomized gratings. The results indicate that the various forms of line variation, with the exception of line edge variation, can have a large effect on the results of scatterometry measurements and interpretation. A mean-field model is suggested that approximates the behavior found in the MC-simulations in a number of different cases. The model is much more computationally efficient, and uses calculation results that would otherwise need to be performed anyway during scatterometry library generation.

5. Acknowledgments

The author would like to thank Drs. Heather Patrick, Krzysztof Michalski, Ravikiran Attota, Robert Larrabee, Egon Marx, and Richard Silver for many useful discussions.

References

1. S. A. Coulombe, B. K. Minhas, C. J. Raymond, S. Sohail, H. Naqvi, and J. R. McNeil, "Scatterometry measurement of sub-0.1 µm linewidth gratings," J. Vac. Sci. Technol. B 16, 80-87 (1998).

2. H.-T. Huang, W. Kong, and F. L. Terry, Jr., "Normal-incidence spectroscopic ellipsometry for critical dimension monitoring," Appl. Phys. Lett. 78, 3983-3985 (2001).

3. P. Lalanne and G. M. Morris, "Highly improved convergence of the couple-wave method for TM polarization," J. Opt. Soc. Am. A 13, 779-784 (1996).

4. J. R. Marciante, N. O. Farmiga, J. I. Hirsh, M. S. Evans, and H. T. Ta, "Optical measurement of depth and duty cycle for binary diffraction gratings with subwavelength features," Appl. Opt. 42, 3234-3240 (2003).

5. B. K. Minhas, S. A. Coulombe, S. S. H. Naqvi, and J. R. McNeil, "Ellipsometric scatterometry for the metrology of sub-0.1-µm-linewidth structures," Appl. Opt. 37, 5112-5115 (1998).

6. M. G. Moharam, E. B. Grann, D. A. Pommet, and T. K. Gaylord, "Formulation for stable and efficient implementation of the rigorous coupled-wave analysis of binary gratings," J. Opt. Soc. Am. A 12, 1068-1076 (1995).

7. M. G. Moharam, D. A. Pommet, E. B. Grann, and T. K. Gaylord, "Stable implementation of the rigorous coupled-wave analysis for surface-relief gratings: enhanced transmittance matrix approach," J. Opt. Soc. Am. A 12, 1077-1086 (1995).

8. X. Niu, N. Jakatdar, J. Bao, and C. J. Spanos, "Specular Spectroscopic Scatterometry," IEEE Trans. Semiconductor Manufacturing 14, 97-111 (2001).

9. C. J. Raymond, M. R. Murnane, S. S. H. Naqvi, and J. R. McNeil, "Metrology of subwavelength photoresist gratings using optical scatterometry," J. Vac. Sci. Technol. B 13, 1484 (1995).

10. C. J. Raymond, M. R. Murnane, S. L. Prins, S. Sohail, H. Naqvi, J. R. McNeil, and J. W. Hosch, "Multiparameter grating metrology using optical scatterometry," J. Vac. Sci. Technol. B 15, 361--368 (1997).

11. V. A. Ukraintsev, "A comprehensive test of optical scatterometry readiness for 65 nm technology production," in *Metrology, Inspection, and Process Control for Microlithography XX*, C. N. Archie, ed., Proc. SPIE 6152, 61521G-1 (2006).

12. W. Yang, J. Hu, R. Lowe-Webb, R. Korlahalli, D. Shivaprasad, H. Sasano, W. Liu, and D. S. L. Mui, "Line-Profile and Critical-Dimension Monitoring Using a Normal Incidence Optical CD Metrology," IEEE Trans. Semiconductor Manufacturing 17, 564-572 (2004).

Tables

Table 1: Average fraction of power diffracted into different orders for normal illumination calculated for line edge variation.

	Order		
	±1	±2	±3
Random edge variation	26 %	16 %	7 %
Line width variation	21 %	16 %	13 %
Line position variation	10 %	21 %	18 %

Figure Captions

Figure 1: Illustration of the four different profile perturbations considered in this study: (a) line edge variation, (b) sidewall roughness, (c) line height variation, and (d) trench depth variation. The greyscale represents the refractive index in the *xz* plane; the profiles are independent of the *y* direction. The profiles shown here are exaggerated, having twice the maximum modulation considered in the simulations. In both (a) and (b), the case of random edge variation is shown.

Figure 2: Specular reflectance Stokes parameters calculated as functions of rms variation σ for normal incidence and for (open symbols) MC-simulated line edge variation, (closed symbols) MC-simulated sidewall roughness, and (curves) the simplified mean-field model. Three cases are shown: (a) random edge variation, (b) line width variation, and (c) line position variation. The symbols and curves represent (squares, solid curves) R_0, (circles, dashed curves) R_1, (upward triangles, dotted curves) R_2, and (downward triangles, dash-dot curves) R_3.

Figure 3: Same as Fig. 2, except for an incident angle of 70°.

Figure 4: Specular reflectance Stokes parameters calculated as functions of rms variation σ for normal incidence and for (a) line height variation and (b) trench depth variation. The data represent (symbols) the MC simulations and (curves) the simplified mean-field model. The symbols and curves represent (squares, solid curves) R_0, (circles, dashed curves) R_1, (upward triangles, dotted curves) R_2, and (downward triangles, dash-dot curves) R_3.

Figure 5: Same as Fig. 4, except for an incident angle of 70°.

Figure 6: Integrated non-specular diffraction efficiency found from MC simulation for normal incidence as a function of rms variation σ for (open symbols) line edge variation, (closed symbols) sidewall roughness. Three cases are shown: (squares) random edge variation, (circles) line width variation, and (triangles) line position variation.

Figure 7: Normal incidence Stokes reflectance as a function of wavelength for (symbols) MC-simulated random line edge variation with σ = 10 nm, (solid curve) unperturbed profile, (dashed curve) the mean-field model, and (dotted curve) the result of a best fit to a simple profile with a non-vertical sidewall, as described in the text.

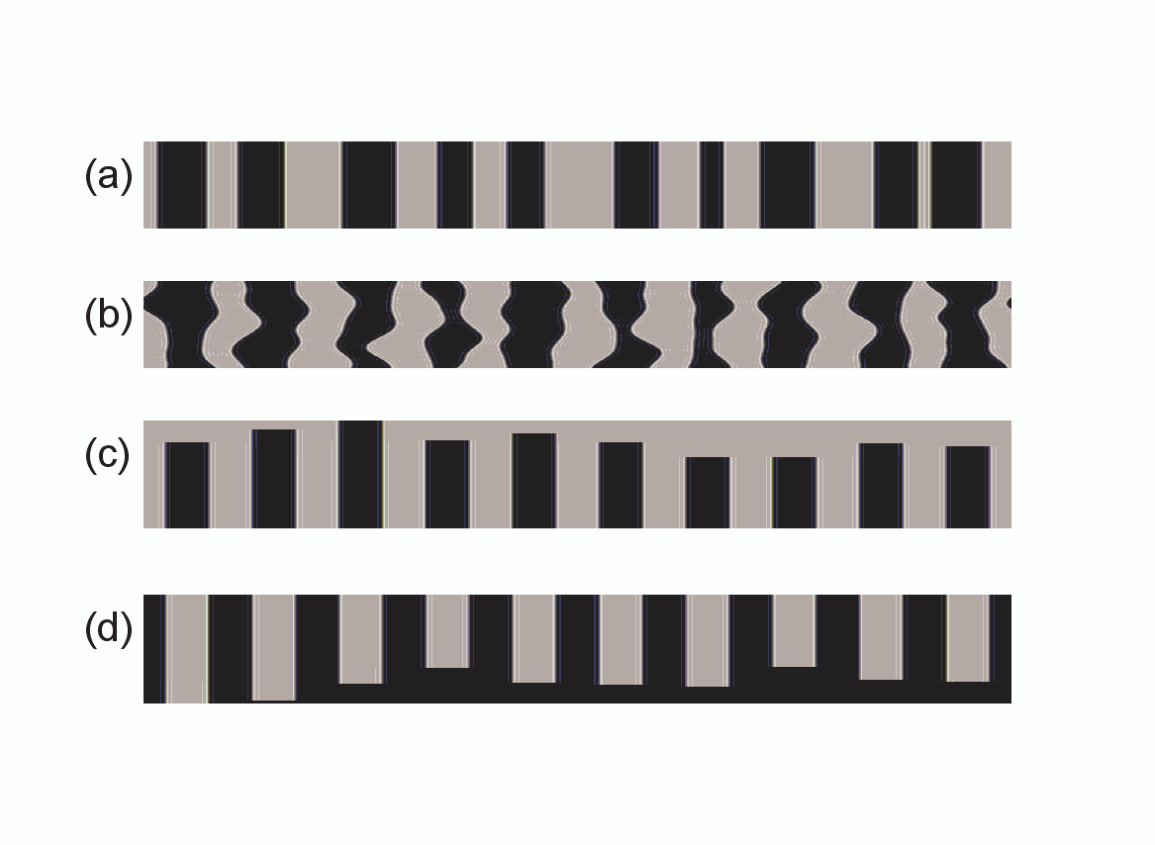

Figure 1: Illustration of the four different profile perturbations considered in this study: (a) line edge variation, (b) sidewall roughness, (c) line height variation, and (d) trench depth variation. The greyscale represents the refractive index in the *xz* plane; the profiles are independent of the *y* direction. The profiles shown here are exaggerated, having twice the maximum modulation considered in the simulations. In both (a) and (b), the case of random edge variation is shown.

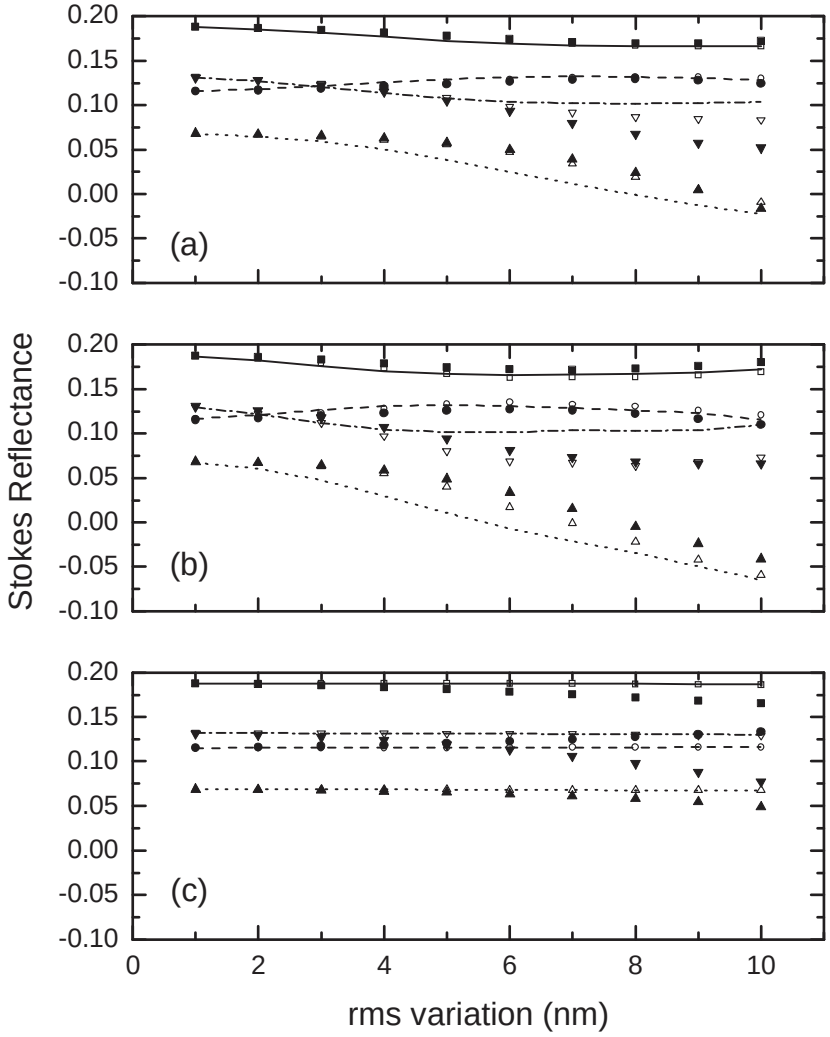

Figure 2: Specular reflectance Stokes parameters calculated as functions of rms variation σ for normal incidence and for (open symbols) MC-simulated line edge variation, (closed symbols) MC-simulated sidewall roughness, and (curves) the simplified mean-field model. Three cases are shown: (a) random edge variation, (b) line width variation, and (c) line position variation. The symbols and curves represent (squares, solid curves) R_0, (circles, dashed curves) R_1, (upward triangles, dotted curves) R_2, and (downward triangles, dash-dot curves) R_3.

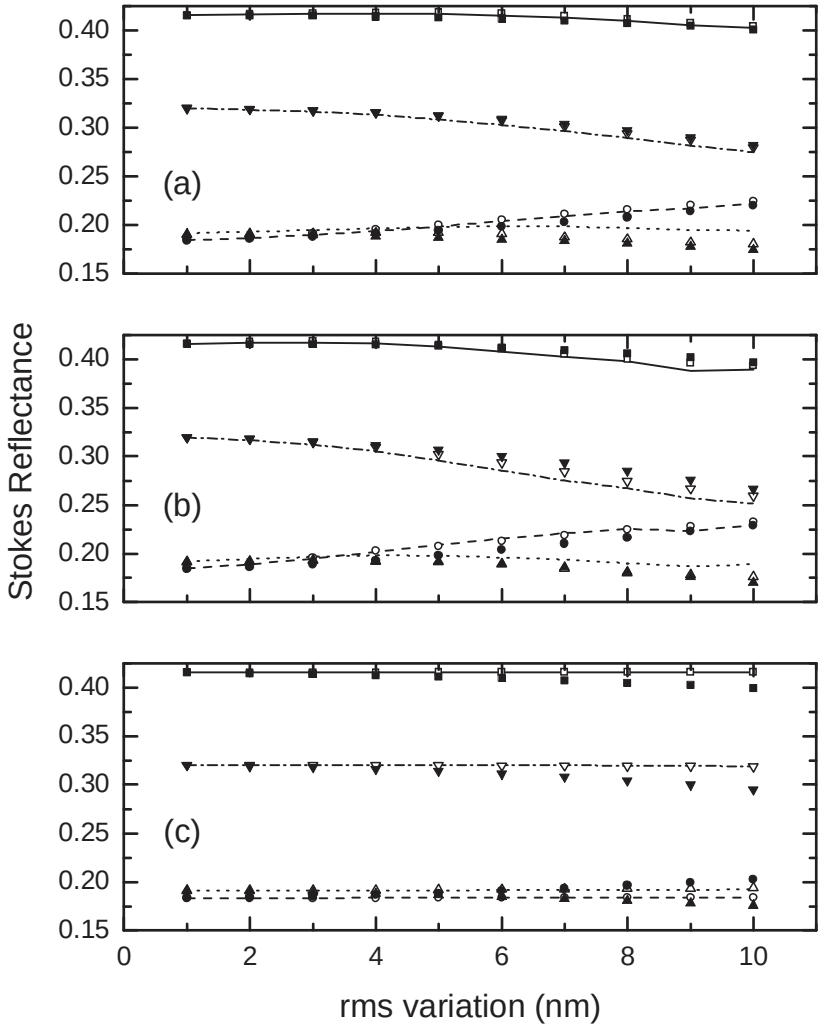

Figure 3: Same as Fig. 2, except for an incident angle of 70°.

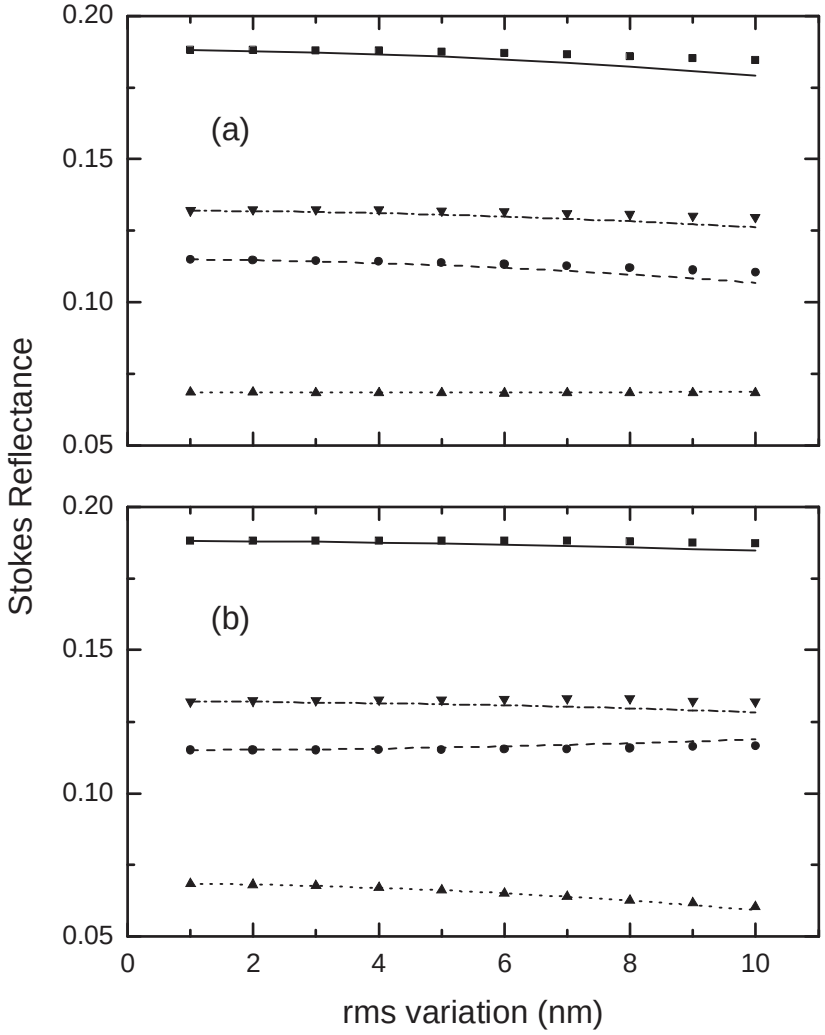

Figure 4: Specular reflectance Stokes parameters calculated as functions of rms variation σ for normal incidence and for (a) line height variation and (b) trench depth variation. The data represent (symbols) the MC simulations and (curves) the simplified mean-field model. The symbols and curves represent (squares, solid curves) R_0, (circles, dashed curves) R_1, (upward triangles, dotted curves) R_2, and (downward triangles, dash-dot curves) R_3.

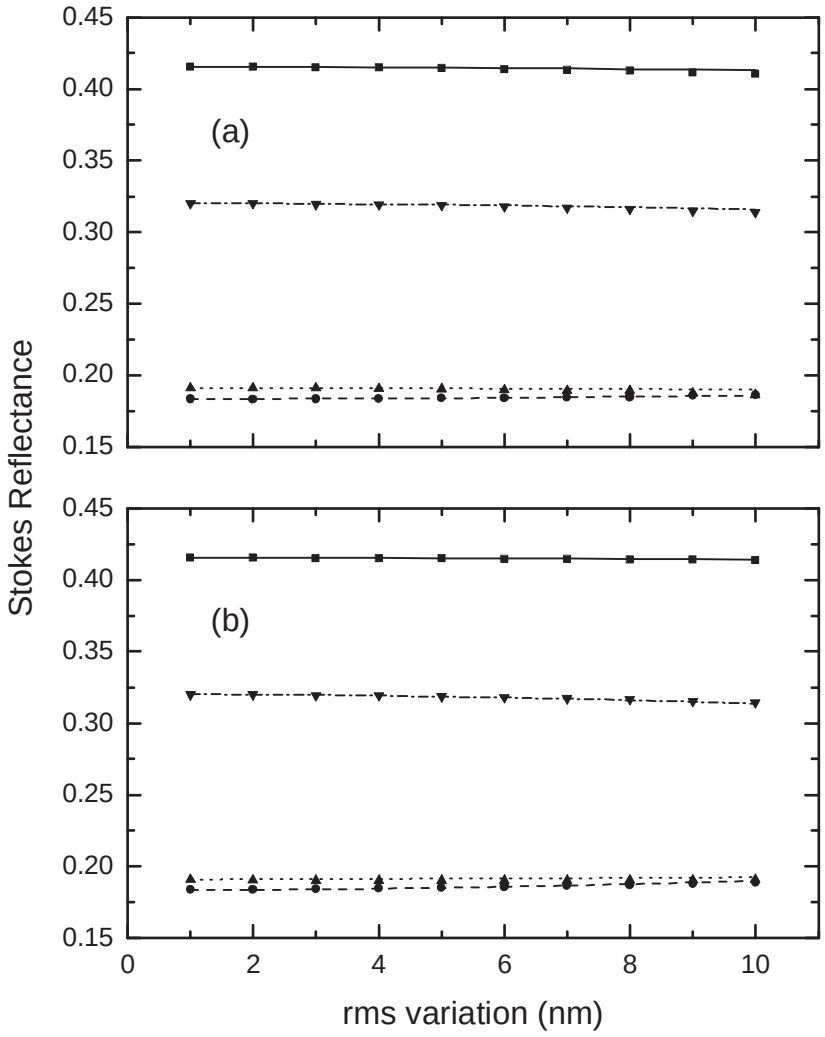

Figure 5: Same as Fig. 4, except for an incident angle of 70°.

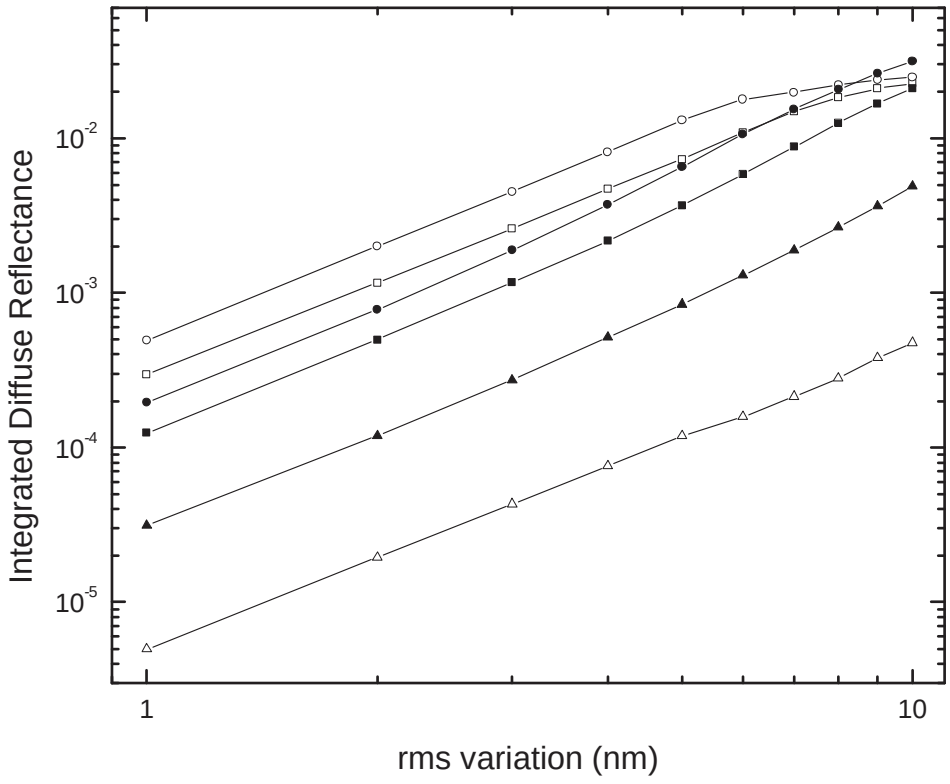

Figure 6: Integrated non-specular diffraction efficiency found from MC simulation for normal incidence as a function of rms variation σ for (open symbols) line edge variation, (closed symbols) sidewall roughness. Three cases are shown: (squares) random edge variation, (circles) line width variation, and (triangles) line position variation.

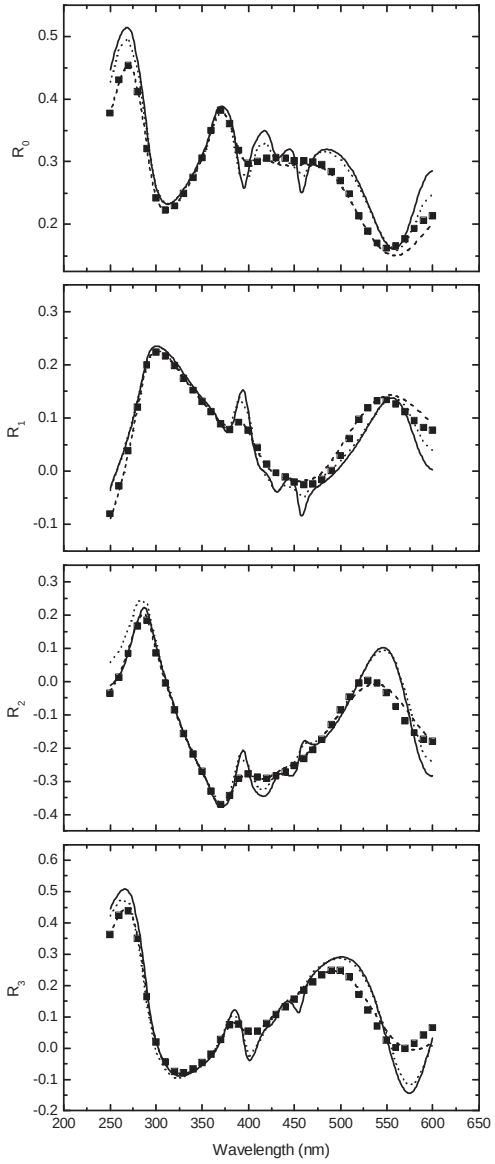

Figure 7: Normal incidence Stokes reflectance as a function of wavelength for (symbols) MC-simulated random line edge variation with σ= 10 nm, (solid curve) the nominal profile, (dashed curve) the mean-field model, and (dotted curve) the result of a best fit to a simple profile with a non-vertical sidewall, as described in the text.